

Synchronization transition from chaos to limit cycle oscillations when a locally coupled chaotic oscillator grid is coupled globally to another chaotic oscillator

Cite as: Chaos **30**, 033121 (2020); <https://doi.org/10.1063/1.5134821>

Submitted: 02 November 2019 . Accepted: 24 February 2020 . Published Online: 12 March 2020

Vedasri Godavarthi, Praveen Kasthuri, Sirshendu Mondal , R. I. Sujith , Nobert Marwan , and Jürgen Kurths 



[View Online](#)



[Export Citation](#)



[CrossMark](#)



CHALLENGE THE IMPOSSIBLE
WITH OUR PRACTICAL REFERENCE GUIDES

Learn more 



Synchronization transition from chaos to limit cycle oscillations when a locally coupled chaotic oscillator grid is coupled globally to another chaotic oscillator

Cite as: Chaos 30, 033121 (2020); doi: 10.1063/1.5134821

Submitted: 2 November 2019 · Accepted: 24 February 2020 ·

Published Online: 12 March 2020



View Online



Export Citation



CrossMark

Vedasri Godavarthi,¹ Praveen Kasthuri,¹ Sirshendu Mondal,²  R. I. Sujith,^{1,a)}  Nobert Marwan,³ 
and Jürgen Kurths^{3,4,5} 

AFFILIATIONS

¹Department of Aerospace Engineering, Indian Institute of Technology Madras, 600036 Chennai, India

²Department of Mechanical Engineering, National Institute of Technology Durgapur, 713209 Durgapur, India

³Potsdam Institute for Climate Impact Research, P.O. Box 60 12 03, 14412 Potsdam, Germany

⁴Department of Physics, Humboldt University, Newtonstr. 15, 12489 Berlin, Germany

⁵Institute for Complex Systems and Mathematical Biology, University of Aberdeen, Aberdeen AB243UE, United Kingdom

^{a)}Author to whom correspondence should be addressed: sujith@iitm.ac.in

ABSTRACT

Some physical systems with interacting chaotic subunits, when synchronized, exhibit a dynamical transition from chaos to limit cycle oscillations via intermittency such as during the onset of oscillatory instabilities that occur due to feedback between various subsystems in turbulent flows. We depict such a transition from chaos to limit cycle oscillations via intermittency when a grid of chaotic oscillators is coupled diffusively with a dissimilar chaotic oscillator. Toward this purpose, we demonstrate the occurrence of such a transition to limit cycle oscillations in a grid of locally coupled non-identical Rössler oscillators bidirectionally coupled with a chaotic Van der Pol oscillator. Further, we report the existence of symmetry breaking phenomena such as chimera states and solitary states during this transition from desynchronized chaos to synchronized periodicity. We also identify the temporal route for such a synchronization transition from desynchronized chaos to generalized synchronization via intermittent phase synchronization followed by chaotic synchronization and phase synchronization. Further, we report the loss of multifractality and loss of scale-free behavior in the time series of the chaotic Van der Pol oscillator and the mean field time series of the Rössler system. Such behavior has been observed during the onset of oscillatory instabilities in thermoacoustic, aeroelastic, and aeroacoustic systems. This model can be used to perform inexpensive numerical control experiments to suppress synchronization and thereby to mitigate unwanted oscillations in physical systems.

Published under license by AIP Publishing. <https://doi.org/10.1063/1.5134821>

During the onset of oscillatory instabilities that occur due to feedback between various subsystems in turbulent systems, we observe a transition from chaos to order. Examples for these are the occurrence of oscillatory instabilities in thermoacoustic, aeroelastic, and aeroacoustic systems. The onset of the oscillatory instabilities in such systems is shown as a transition from chaos to limit cycle oscillations via intermittency.¹⁻³ Further, the synchronization framework has been applied to describe the onset of thermoacoustic and aeroelastic instabilities. The onset of thermoacoustic instabilities is described as the occurrence of

synchronization between the acoustic field and the global heat release rate in a turbulent combustor.⁴ The onset of aeroelastic instability in a pitch-plunge aeroelastic system is described as the onset of synchronization between the pitch and the plunge modes.⁵ Further, a spatiotemporal transition from disorder to order via a chimera-like state is detected.^{6,7} Such systems with many interacting subunits are generally modeled using a grid of oscillators. However, the transition in the dynamics from chaos to limit cycle oscillations among chaotic oscillators has been observed only with conjugate coupling or time delay coupling.

Here, we show that this transition to limit cycle oscillations is also possible when different chaotic oscillators are coupled. We show an alternate route wherein a transition from chaos to limit cycle oscillations occurs when a grid of locally coupled Rössler oscillators is bidirectionally coupled with a chaotic Van der Pol (VDP) oscillator. We explore the temporal and spatiotemporal synchronization route to limit cycle oscillations. We further draw some analogies between the model in our study with the experimental results from thermoacoustic and aeroelastic systems. Models such as ours can be used to perform inexpensive numerical control experiments to suppress the limit cycle oscillations having ruinously large amplitudes observed during the occurrence of oscillatory instabilities in such systems.

I. INTRODUCTION

The emergence of collective behavior through synchrony among coupled subunits of individual components is observed in many biological,^{8–10} physical,¹¹ chemical,^{12–14} and engineering^{15,16} systems. Such systems can be modeled using a network of oscillators and the dynamics exhibited depends on the type of oscillators, the topology over which the oscillators are arranged, the type of coupling, and the number of oscillators.^{17,18} Quite generally, as the coupling strength among the oscillators is increased, the system transitions from an asynchronous state to a synchronous state.¹⁹ During this transition, the existence of symmetry breaking states such as chimera states²⁰ and solitary states²¹ received a lot of attention due to their applications in physical and biological systems. The co-existence of phase synchronous and asynchronous regions is referred to as a chimera state.²⁰ In contrast, for a solitary state, one or more oscillators oscillate with different mean frequencies than the other oscillators.²¹

Despite a large number of studies on network of oscillators, very few studies focused on the transition from chaos to limit cycle oscillations via intermittency. The transition from chaos to limit cycle oscillations in the case of chaotic oscillators is generally observed when time delay coupling is introduced²² or when coupled conjugatively.²³ Karnatak *et al.*²³ reported the route to chaos suppression among dissimilarly coupled Rössler oscillators as a transition from desynchronization to generalized synchronization (GS) via phase synchronization (PS). Chaurasia and Sinha²⁴ also reported the suppression of chaos when nonidentical chaotic oscillators are coupled. They observed the transition from chaos to a stable fixed state when a grid of Rössler oscillators is coupled with the Lorenz oscillator and this transition is not seen when identical chaotic oscillators are coupled. In this study, we demonstrate the transition from chaos to limit cycle oscillations via intermittency when two dissimilar chaotic oscillators are coupled. Further, we report the existence of both intermittent phase synchronization and phase synchronization during the transition from desynchronization to generalized synchronization when two different types of chaotic oscillators are coupled without incorporating time delay or conjugate coupling. We further report the presence of various symmetry breaking phenomena during this transition.

A transition from chaotic oscillations to limit cycle oscillations via intermittency is observed among physical systems mainly

during the self-organization of turbulent flows in plasma turbulence and transitions to oscillatory instabilities such as thermoacoustic,²⁵ aeroelastic,²⁶ and aeroacoustic instabilities in turbulent systems. Thermoacoustic instability, a serious problem faced by gas turbine engines and rocket motors,²⁷ occurs due to the positive feedback between the acoustic field in the confinement and the unsteady heat release rate in combustors. Similarly, aeroelastic flutter occurs due to the feedback between the fluctuations in the fluid flow and the structural modes. This fluid–structure interaction is observed when the aerodynamic forces overcome the elastic and inertial forces of an elastic structure in the flow field.²⁸ Thermoacoustic and aeroelastic instabilities are comprised of self-excited large amplitude periodic oscillations which are detrimental to the structural integrity of the engine²⁷ and aircraft wings,^{5,26} respectively. Such transitions are due to synchronization between two different chaotic subsystems of the respective turbulent systems. In the case of a thermoacoustic system,⁴ the acoustic field and the unsteady heat release rate synchronize, whereas in the case of an aeroelastic system consisting of an airfoil with pitch-plunge degrees of freedom,⁵ the pitch and plunge modes synchronize. Both these studies reported the synchronization transition as a transition from desynchronized chaos to synchronized periodicity via intermittent phase synchronization and phase synchronization. Further, Mondal *et al.*⁶ reported a spatiotemporal transition from desynchronized disorder to synchronized order via chimera-like states during the transition to thermoacoustic instability. Recently, Dutta *et al.*²⁹ proposed a Kuramoto model to capture the dynamics in a swirl stabilized combustor en route to thermoacoustic instability. They modeled each flamelet in a swirl combustor as a Kuramoto oscillator. They increased the coupling between the oscillators, which is analogous to the coupling between the flamelets in a combustor, thereby obtaining similar dynamics as that of a swirl stabilized combustor. However, it is important to capture the temporal and spatiotemporal synchronization route to thermoacoustic instability, which occurs due to the mutual synchronization between two different oscillators, i.e., the acoustic field and the turbulent reactive flow in a combustor.

In this work, we attempt to capture the transition from chaos to limit cycle oscillations in a model problem where a network of locally coupled Rössler oscillators is bidirectionally coupled with a dissimilar oscillator, the chaotic Van der Pol (VDP) oscillator. The intermittency route to limit cycle oscillations is not trivial among dissipatively coupled chaotic oscillators as they undergo chaotic synchronization. Here, the transition to limit cycle oscillations occurs as the coupling between the Rössler system and VDP oscillator is strengthened. In other words, the coupling with the chaotic VDP oscillator induces the transition from chaos to limit cycle oscillations. Recently, Meena *et al.*³⁰ reported the existence of chimera states in star networks when the hub node and the other nodes are dissimilar oscillators, i.e., when a system of identical oscillators is externally coupled with dissimilar oscillators. Since we have a similar system where the chaotic VDP oscillator is externally coupled to the Rössler oscillators, we expect the presence of symmetry breaking states. We also report the existence of symmetry breaking phenomena such as intermittent partial synchronization, chimera states, and solitary states during this transition. We show similarities in the dynamics observed in the model with experimental results obtained during the transition to thermoacoustic^{1,4,6} and aeroelastic^{3,5}

instabilities in turbulent systems. We stress the similarity of behavior observed in the transition to oscillatory instability in a complex thermoacoustic system with that observed when dissimilar chaotic oscillators are coupled. The findings we discuss are not limited to Rössler–Van der Pol system but can also be observed with a different external oscillator such as a modified Duffing oscillator, which has a tendency to transition from chaos to limit cycle oscillations on forcing. We show the intermittency route to limit cycle oscillations in both Rössler–chaotic VDP and Rössler–chaotic Duffing systems in [Appendix B](#). The model described in this work also facilitates a new perspective in controlling the oscillatory instabilities. The problem of controlling oscillatory instabilities can be posed as a disruption of synchronization among the oscillators. This perspective of viewing the transition to oscillatory instabilities as coupled interaction of oscillators provides a wide range of tools to conduct numerical control experiments targeted at disrupting synchronization.

The rest of the paper is organized as follows. The model consisting of the grid of Rössler oscillators and the chaotic VDP oscillator is described in [Sec. II](#), followed by results and discussions in [Sec. III](#). The conclusions are given in [Sec. IV](#).

II. MODEL

The model comprises of a square grid of N Rössler oscillators, which are diffusively coupled [Eq. (1)] and a chaotic VDP oscillator [Eq. (2)],

$$\begin{aligned} \dot{x}_i &= -w_i y_i - z_i, \\ \dot{y}_i &= w_i x_i + a y_i + \mu_{vy} (v - y_i) + \mu_{yy} \sum_{j \in \delta(y_i)} (y_j - y_i), \end{aligned} \quad (1)$$

$$\dot{z}_i = b + z_i (x_i - c),$$

$$\dot{u} = v,$$

$$\dot{v} = 0.1 (1 - u^2) v - u^3 + \cos t + \mu_{yv} \sum_{k=1}^N (y_k - v), \quad (2)$$

where $a = 0.165$, $b = 0.2$, and $c = 10$ are the parameters of the individual Rössler oscillators. $\delta(y_i)$ represents the nearest neighborhood of the i th Rössler oscillator and N represents the total number of Rössler oscillators. The ordinates of these oscillators are coupled to their neighbors within a distance of $\sqrt{2}$ units, with a coupling strength of μ_{yy} (intra-Rössler coupling). The natural frequencies of individual Rössler oscillators (w_i) are assigned randomly from a Gaussian distribution with a mean of around 0.8 and a standard deviation of 0.05. Equation (B2) represents a chaotic VDP oscillator.³¹ The second coordinates of the Rössler system (y) and the chaotic VDP oscillator (v) are bidirectionally coupled with strengths of μ_{vy} and μ_{yv} , which corresponds to the influence of the VDP oscillator on a Rössler oscillator and vice versa.

We see the transition from chaotic to limit cycle oscillations during the onset of oscillatory instabilities in turbulent systems. The spatiotemporal transition has also been studied extensively during the transition to thermoacoustic instability in a turbulent combustor. This can be further extended to other oscillatory instabilities

such as aeroelastic and aeroacoustic instabilities that occur during the self-organization of turbulent flows. We, therefore, compare various aspects of the model [Eqs. (1) and (2)] with those observed in a turbulent combustor. We further choose the relations among the coupling strengths μ_{yy} , μ_{yv} , and μ_{vy} accordingly. Each chaotic Rössler oscillator is analogous to the local heat release rate oscillations. The complexities due to the underlying turbulent flow result in the variation of natural frequencies among these oscillators. Hence, we chose non-identical Rössler oscillators by incorporating differences in w_i . We hypothesize that the coupling strength μ_{yy} quantifies an interaction analogous to the interaction between the local heat release rate oscillations, which occurs through the process of turbulent diffusion during combustion. The chaotic VDP oscillator is analogous to the global acoustic field and hence is coupled to each Rössler oscillator. Moreover, in our earlier study, we reported that the unsteady flame dynamics exerts a stronger influence on the acoustic field than vice versa.³² Hence, we vary μ_{yv} and μ_{vy} as per the relation $\mu_{yv} = 1.2\mu_{vy}$. As the synchronization between the heat release rate oscillations and the acoustic pressure fluctuations occurs, there is an emergence of coherent structures in the flow field which enhances the interaction among the local heat release rate oscillations. Therefore, we use a proportional relationship between μ_{vy} and μ_{yv} as $\mu_{yv} = 0.1\mu_{vy}$. We observe a transition from chaos to limit cycle oscillations as μ_{vy} (hereon denoted as μ for convenience) is increased from 0 to 0.5. Thus, as the coupling strength (μ) is increased, we observe synchrony among the Rössler oscillators along with the synchronization between the set of Rössler oscillators and chaotic VDP oscillator.

III. RESULTS

The set of equations, Eqs. (1) and (2), is integrated using the fourth order Runge–Kutta method with a time step of $dt = 10^{-3}$. μ is varied from 0 to 0.5 in steps of 0.001. In this study, the analysis is performed for a 10×10 square grid of Rössler oscillators and thus $N = 100$. The initial conditions for the set of Rössler equations are [1, 1, 1] and the initial conditions of the chaotic VDP oscillator are [0, 0]. We remove an initial transience of 100 time units from the solution. Here, the mean subtracted ordinate (v') of the chaotic VDP oscillator represents the fluctuations in the acoustic field in a turbulent combustor. The fluctuations in the mean field (\bar{y}') of the ordinate of Rössler system are analogous to the fluctuations in the global heat release rate in a thermoacoustic system. We characterize the temporal synchronization transition using (v') and (\bar{y}'). The results are independent of the grid size for $N \geq 100$ (see [Fig. 6](#) in [Appendix A](#)).

A. Analysis of temporal transition from chaos to limit cycle oscillations

For $\mu \leq 0.01$, we observe aperiodic fluctuations in v' and \bar{y}' and they appear to oscillate independently [[Fig. 1-I\(a\)](#)]. As μ is increased from 0.01 to 0.03, short bursts of weakly periodic oscillations appear amid aperiodic oscillations [[Fig. 1-I\(b\)](#)]. This state is similar to the intermittency state, where bursts of periodic oscillations appear amidst aperiodic epochs at random intervals.¹ This

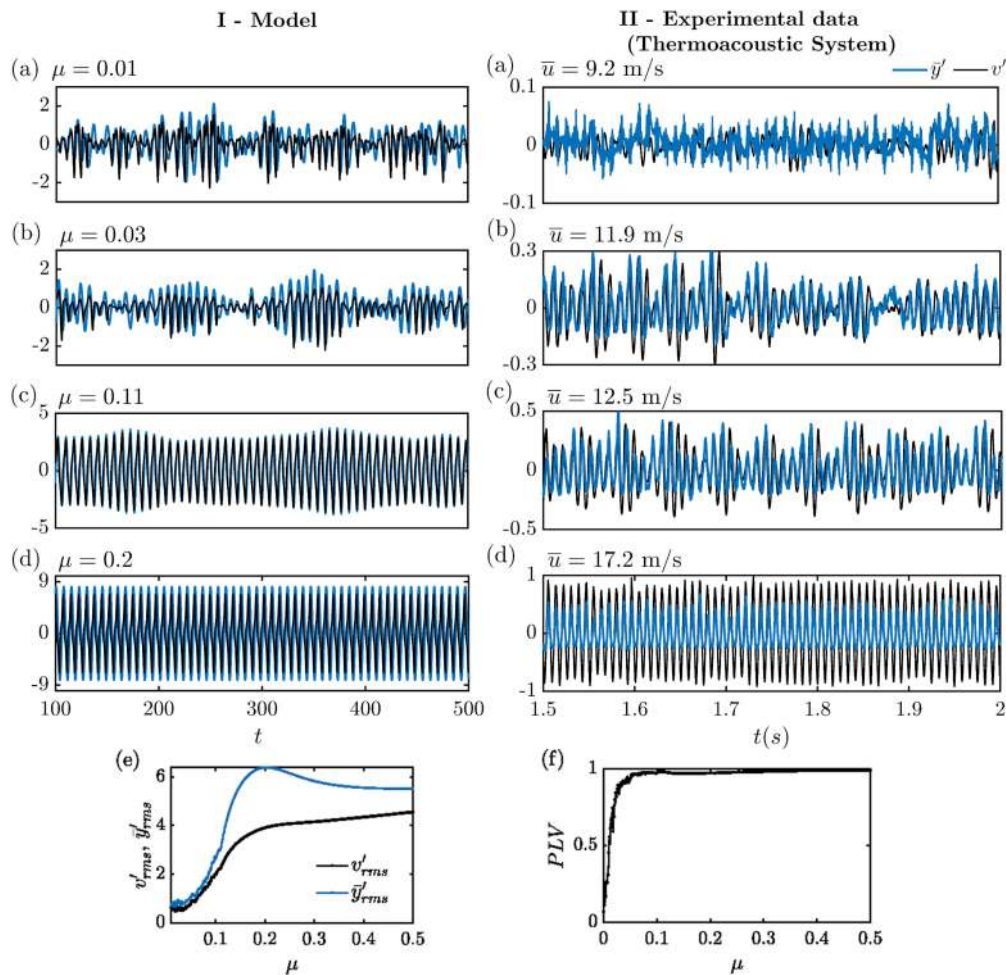


FIG. 1. I(a)–(d) Time series of v' and \bar{y}' of model obtained at $\mu = 0.01, 0.03, 0.11,$ and 0.2 . II(a)–(d) Time series of the acoustic pressure (v') and global heat release rate (\bar{y}') obtained in experiments from a thermoacoustic system, a turbulent combustor, at air flow velocities $\bar{u} = 9.2, 11.9, 12.5,$ and 17.2 m/s. These data are presented in Ref. 32. Reproduced with permission from Godavarthi *et al.*, *Chaos* **28**, 113111 (2018). Copyright 2018 AIP Publishing LLC. (e) Variation of rms values of v' and \bar{y}' from the model with μ . (f) Phase locking value (PLV) of v' and \bar{y}' from the model.

intermittency is in contrast with the general definition of intermittency, where we observe bursts of large amplitude aperiodic oscillations amidst low amplitude periodic oscillations.³³ On further increase in μ , the duration and the amplitude of these bursts increase. As μ approaches 0.11, we observe that both v' and \bar{y}' oscillate periodically. We also find amplitude modulation in the signal [Fig. 1-I(c)]. The presence of amplitude modulation in the pressure and global heat release rate signals obtained in experiments can be seen in Pawar *et al.*⁴ and Nair *et al.*¹ The reason for the amplitude modulation is the presence of slow scale oscillations in the system.³⁴ This amplitude modulation in the oscillations disappears for $\mu > 0.11$ [Fig. 1-I(d)]. In short, the temporal transition occurs from chaos to large amplitude limit cycle oscillations via intermittency and a periodic oscillation with amplitude modulation. This transition is similar to that experimentally observed during the transition

to thermoacoustic, aeroelastic and aeroacoustic instabilities^{1,2,4,26} and can be clearly seen in Fig. 1-II(a)–(d).

Further, we observe an increase in root mean square (rms) values in v' and \bar{y}' with μ [Fig. 1(e)]. The rms of a mean subtracted signal v' sampled at M intervals is given by $\sqrt{\frac{1}{M} \sum_{i=1}^M (v'_i)^2}$. We observe some fluctuations in the variation of v'_{rms} , \bar{y}'_{rms} until $\mu = 0.1$ due to the presence of both periodic and aperiodic oscillations. On further increase in μ , there is a monotonic increase in v'_{rms} and \bar{y}'_{rms} . Beyond $\mu = 0.2$, \bar{y}'_{rms} decreases mildly and saturates after a coupling strength of $\mu = 0.4$. We next quantify the synchrony between v' and \bar{y}' for various values of μ using phase locking value (PLV) [Fig. 1(f)].

We denote the instantaneous phases of the two signals v' and \bar{y}' sampled at M instants by $\phi_v(t)$ and $\phi_y(t)$, respectively. The

instantaneous phases of the signal $v(t)$ are computed using the Hilbert transform of the original signal, $v_H(t)$.³⁵ Then, the PLV of the signals $v(t)$ and $\bar{y}(t)$ is given by $\frac{1}{M} \left| \sum_{i=1}^M e^{j(\phi_{v(t_i)} - \phi_{\bar{y}(t_i)})} \right|$, where, $j = \sqrt{-1}$. PLV takes a value between 0 and 1, where 0 indicates that the oscillators are desynchronized and 1 indicates that the oscillators are phase synchronized.³⁵

PLV shows a steep increase until $\mu = 0.03$ [Fig. 1(f)]. This is reflected as an intermittency state in the v' and \bar{y}' oscillations in Fig. 1-I(b). PLV attains a value closer to 1 when $\mu = 0.07$, indicating the onset of phase synchronization between v' and \bar{y}' . For further change in μ , we observe that PLV stays close to 1.

1. Characterization of synchronization route to limit cycle oscillations

We characterize the type of synchronization behavior at various values of μ using the plots of the probability of recurrence $P(\tau)$ as a function of τ in Fig. 2] of v' and \bar{y}' . Recurrence is a fundamental property of any deterministic dynamical system.³⁶ Recurrence is the tendency of a trajectory in phase space to revisit the same neighborhood after a certain time. $P(\tau)$ measures the probability with which a trajectory in phase space (X_i) revisits the same neighborhood after a

time lag τ and is given as³⁷ $P(\tau) = \frac{1}{N-\tau} \sum_{i=1}^{N-\tau} \Theta(\epsilon - \|X_i - X_{i+\tau}\|)$, where Θ is the Heaviside function. In this study, we use a modified form of $P(\tau)$ proposed by Goswami *et al.*³⁸ and consider only those lags (τ) which are greater than the lag (τ_c) at which the autocorrelation of the signal is lesser than $1/e$ to exclude effects of autocorrelation.

At $\mu = 0.01$ [Fig. 2-I(a)], we observe a very low probability of recurrence $P(\tau)$ of both v' and \bar{y}' since there is no correlation between them, indicating a desynchronized state when $\mu = 0.01$. At higher coupling strengths of around 0.07 [Fig. 2-I(b)], we observe moderate values in $P(\tau)$ of v' and \bar{y}' . However, $P(\tau)$ decays for higher time lags. Nevertheless, the location of the peaks in the plots of $P(\tau)$ coincides, indicating the presence of chaotic phase synchronization (chaotic PS).³⁷ Figure 2-I(c) shows a probability of recurrence close to 1 for both v' and \bar{y}' oscillations at $\mu = 0.1$. Further, the locations of the peaks in the plots of $P(\tau)$ coincide; however, there is a slight mismatch in the amplitude of the peaks. This indicates phase synchronization (PS) and the onset of periodicity in v' and \bar{y}' oscillations.^{37,39} When $\mu = 0.2$, we observe that both the amplitude and location of the peaks in the plots of $P(\tau)$ of v' and \bar{y}' coincide, indicating a generalized synchronization (GS) state.³⁹ The peaks in the plot of $P(\tau)$ of two oscillators coincide when they are in a complete synchronization state; however, since the oscillators in

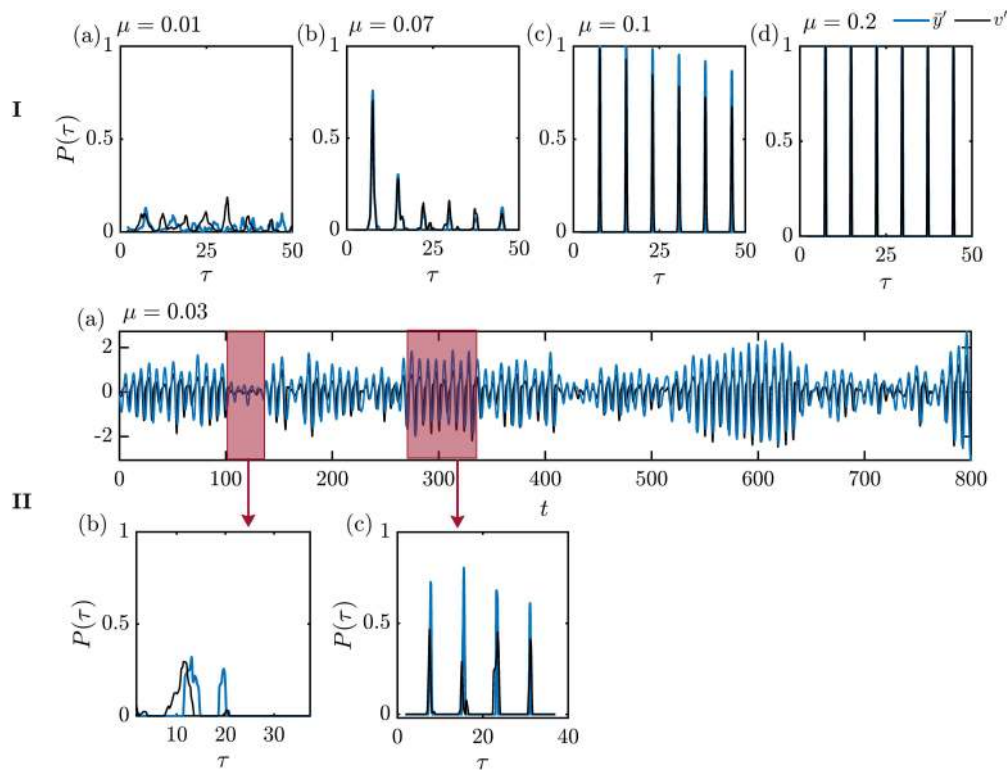


FIG. 2. I(a)–(d) Probability of recurrence, $P(\tau)$, of v' and \bar{y}' fluctuations at $\mu = 0.01, 0.07, 0.1$, and 0.2 , respectively. II(a) Time series during intermittency at $\mu = 0.03$. (b) $P(\tau)$ plots of v' and \bar{y}' during the aperiodic part of intermittency. (c) $P(\tau)$ plots of v' and \bar{y}' during a periodic epoch of intermittency. The embedding dimension and the time delay used for phase space reconstruction are 8 and $\tau_c = 35$ time units. The probability of recurrence, $P(\tau)$, is computed for a window length of 1000 data points, by fixing the recurrence rate at 0.08.

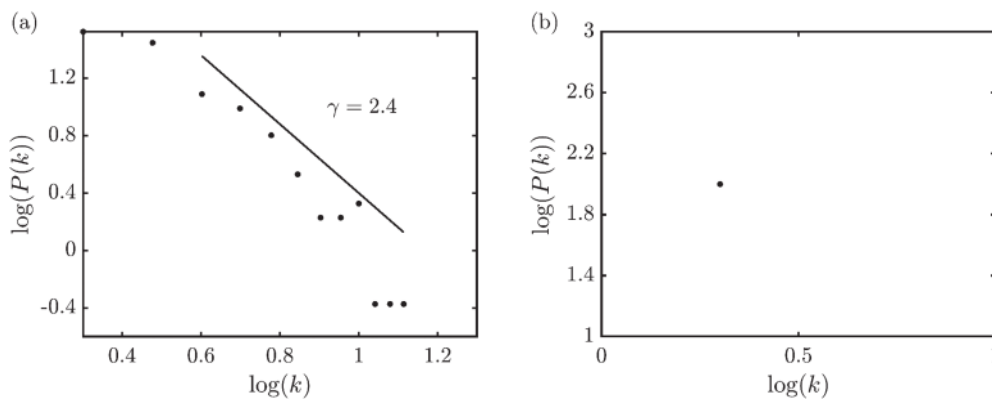


FIG. 3. (a) and (b) Logarithmic plots of $P(k)$ and k constructed from v' during the (a) chaotic and (b) periodic state. We observe that the degree distribution follows a power law with an exponent of 2.4, indicating the presence of scale-free behavior ($\mu = 0.01$). At higher coupling strengths, when the periodic state is reached ($\mu = 0.2$), we observe that the degree distribution collapses to a single point.

hand are non-identical (i.e., one is the ordinate of the mean field of Rössler oscillators and the other is the ordinate of the chaotic VDP oscillator), they are in the GS state.

During intermittency ($\mu = 0.03$), since the v' and \bar{y}' fluctuations comprise of both bursts of weakly periodic oscillations and epochs of aperiodic fluctuations, we analyze these two regimes separately as shown in Fig. 2-II(a)–(c). During an epoch of aperiodic fluctuations, the plots of $P(\tau)$ show a very low value of around 0.2 [Fig. 2-II(b)]. Further, there is a mismatch in the amplitude and the location of the peaks in the plots of $P(\tau)$ of both v' and \bar{y}' indicating asynchrony. During the bursts of periodic oscillations [Fig. 2-II(c)], we observe that the location of the peaks match but the amplitudes do not, indicating the presence of phase synchronized behavior. The existence of asynchrony during the aperiodic part and the phase synchronized behavior during the periodic bursts are characteristic features of an intermittent phase synchronized state (IPS).

In summary, as μ is varied from 0.01 to 0.5, we observe a transition from desynchronized aperiodicity to IPS to chaotic PS followed by PS and GS. Pawar *et al.*⁴ and Raaj *et al.*⁵ reported a similar transition from desynchronized state to IPS followed by PS and GS during the onset of thermoacoustic and aeroelastic instabilities, respectively.

In Secs. III A 2 and III A 3, we explore the route to this synchronization transition using visibility graph and multifractal analysis.

2. Loss of scale-free behavior during synchronization transition

Lacasa *et al.*⁴⁰ developed a methodology of the construction of a network from time series using visibility graphs. In order to construct a visibility graph from a time series $v'(t)$, we consider the sequence of peaks h_k . Visibility graph is a set of nodes and links, where each node represents a peak h_k in the time series and two such peaks are connected with a link if they satisfy the visibility criterion. The information related to nodes and links is encoded in an

adjacency matrix A_{lm} . If two nodes l and m are connected, A_{lm} is one; otherwise A_{lm} is zero. The visibility criterion is given by

$$A_{lm} = \begin{cases} 1 & \text{if } h_k < h_l + (h_m - h_l) \frac{t_k - t_l}{t_m - t_l}, \\ 0 & \text{otherwise,} \end{cases} \quad (3)$$

where k is an intermediate node between l and m (i.e., $l < k < m$) and h_l is the peak value of l th node.

The degree of a node k is determined by the number of nodes that are connected to a given node. The fraction of nodes with a degree k is given by $P(k)$. The type of degree distribution determines the type of the network. For instance, the degree distribution of a random network follows a Poisson distribution.⁴¹ A power law degree distribution $P(k) = k^{-\gamma}$ with $2 < \gamma < 3$ indicates the presence of scale-free behavior.

We construct a visibility graph using v' . Figure 3(a) shows a power law degree distribution in the visibility network constructed from v' when $\mu = 0.01$. The power law exponent is 2.4, which indicates the presence of a scale-free (i.e., scale invariance) behavior during the desynchronized state. On increasing the coupling strength, at $\mu = 0.2$, we observe that the degree distribution collapses to a point from a power law degree distribution, indicating the presence of periodic behavior in v' [Fig. 3(b)]. When $\mu = 0.2$, the degree of all the peaks is 2, indicating that each peak is connected only to its direct neighbors. Thus, we can describe the transition from chaos to limit cycle oscillations as a loss of scale-free behavior. Murugesan and Sujith¹² also described the transition to thermoacoustic instability as a loss of scale-free behavior. They observed that the power law exponent is around 2.5–2.7 (± 0.1) during combustion noise for different configurations of turbulent combustors, i.e., bluff-body stabilized and swirl stabilized combustors.

3. Loss of multifractality during the onset of limit cycle oscillations

Multifractal description of a signal provides a peek into characterizing the complexity of the signal. The concept of a

“fractal” is introduced to describe the objects which exhibit self-similarity at different scales.⁴³ For fractal objects, one cannot determine measures such as length and area, as these quantities depend on the scale of resolution. For example, the dimension of a straight line is 1, but there is no integer dimension for a coastline with wrinkles, as the length of the coastline depends on the scale of magnification.⁴⁴ The fractal dimension for fractal curves varies between 1 and 2. The logarithmic plot of the length of the fractal curve measured with different scales will be a straight line with a negative slope, and the magnitude of this slope is the fractal dimension.

Similar to a fractal object, we observe self-similarity at various time scales in a fractal time series. In some signals, the scaling behavior is complex where the scaling exponent depends on the amplitude of fluctuations. These signals are called multifractal signals. Characterizing such signals using a single scaling exponent is not possible.⁴⁵ The scaling exponent is called the Hurst exponent and we need to determine multiple generalized Hurst exponents for different orders of fluctuations. We estimate the generalized Hurst exponents of a signal by using the multifractal spectrum $f(\alpha)$ vs α (where α is a singularity exponent) computed with the multifractal detrended fluctuation analysis (MFDFA). We provide a brief description of MFDFA in Appendix C.

We observe the presence of multifractal behavior during lower coupling strengths $\mu = 0.03$ in both v' and \bar{y}' signals. However, the multifractal spectrum collapses to a point at $\mu = 0.11$. Thus, we observe a loss of multifractality during the synchronization transition (Fig. 4). This is in accordance with the description of the onset of thermoacoustic instability as a loss of multifractality provided by Nair *et al.*²⁵ and Unni and Sujith.⁴⁶

Until now, we analyzed the temporal behavior during the transition from chaos to limit cycle oscillations. We now investigate the spatiotemporal behavior during the transition.

B. Analysis of spatiotemporal synchronization transition

Kuramoto⁴⁷ introduced an order parameter to quantify the amount of coherence present among the oscillators in a network for a given instant. It is given by $r(t) = \frac{1}{N} \left| \sum_{i=1}^N e^{i\theta_i(t)} \right|$, where N is the total number of oscillators in the network, θ_i is the instantaneous phase difference between i th Rössler oscillator and the chaotic

VDP oscillator, $j = \sqrt{-1}$. The instantaneous phases are computed from a time series using the Hilbert transform. If the instantaneous phase of the i th Rössler oscillator is $\phi_i(t)$ and that of the chaotic VDP is $\phi_v(t)$ obtained through the Hilbert transforms of the respective time series $y_i(t)$ and v' , then $\theta_i = \phi_i(t) - \phi_v(t)$. The order parameter $r(t)$ varies between 0 and 1. A $r(t)$ value of 0 indicates an asynchronous state, whereas a $r(t)$ value of 1 indicates a completely synchronous state. We observe that the time averaged order parameter (\bar{r}) increases with an increase in μ . \bar{r} attains a value closer to 1 at $\mu = 0.2$, indicating an almost complete synchronization among all the 100 Rössler oscillators and the chaotic VDP oscillator (Fig. 5-1).

Chimera states are identified by plotting the mean phase velocities⁴⁸ (ω_i) and the space-time plots of $\cos(\theta_i)$. The mean phase velocity of i th oscillator (ω_i) is computed as $\omega_i = \frac{2\pi S_i}{\Delta T}$, where S_i is the number of complete rotations around the origin performed by the i th oscillator in the time interval ΔT . When ω_i is plotted, the region of constant ω_i corresponds to a synchronous region. The simultaneous existence of constant ω_i and dispersed values of ω_i shows the presence of a chimera state [similar to the variation shown in Fig. 5-II(c)]. Similarly, the variation of $\cos(\theta_i)$ with time gives a peek into the temporal variation. A $\cos(\theta_i)$ value of 1 indicates a synchronization between the Rössler and the chaotic Van der Pol oscillator. A similar temporal $\cos(\theta_i)$ among the oscillators indicates synchrony in the Rössler system.

We observe that for $\mu = 0.01$ [Figs. 5-II(a) and 5-III(a)], the distribution of ω_i and the instantaneous phases are scattered, indicating asynchrony. For $\mu \approx 0.09$ [Fig. 5-II(b)], the Rössler oscillators with close natural frequencies (ω_i) have similar ω_i s. The behavior in the plot of ω_i indicates the presence of clusters which are synchronized. This can be visualized clearly in space-time plots. We observe some small cluster-like structures, such as the one highlighted by a white ellipse during some time intervals [Fig. 5-III(b)]. We find that a few oscillators alternate between the synchronized and desynchronized states. Further, there are some Rössler oscillators which are in-phase synchronized and others which are anti-phase synchronized with the chaotic VDP oscillator. This indicates the presence of intermittent partial synchronization among the Rössler oscillators. At $\mu = 0.11$ [Figs. 5-II(c) and 5-III(c)], we observe that most of the Rössler oscillators are synchronized, while some of them have different mean phase velocities. This indicates the presence of a chimera-like state. As we increase μ , more oscillators synchronize and at $\mu = 0.2$ [Figs. 5-II(d)

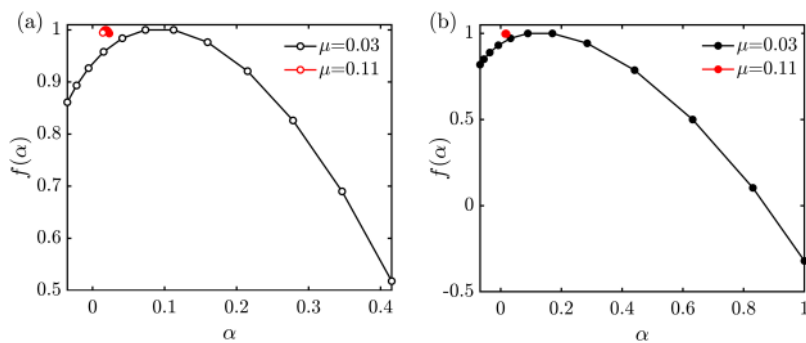


FIG. 4. (a) and (b) $f(\alpha)$ vs α of (a) \bar{y}' and (b) v' at $\mu = 0.03$ and 0.11. We observe that the multifractal spectrum collapses into a point at the onset of limit cycle oscillations in both v' and \bar{y}' .

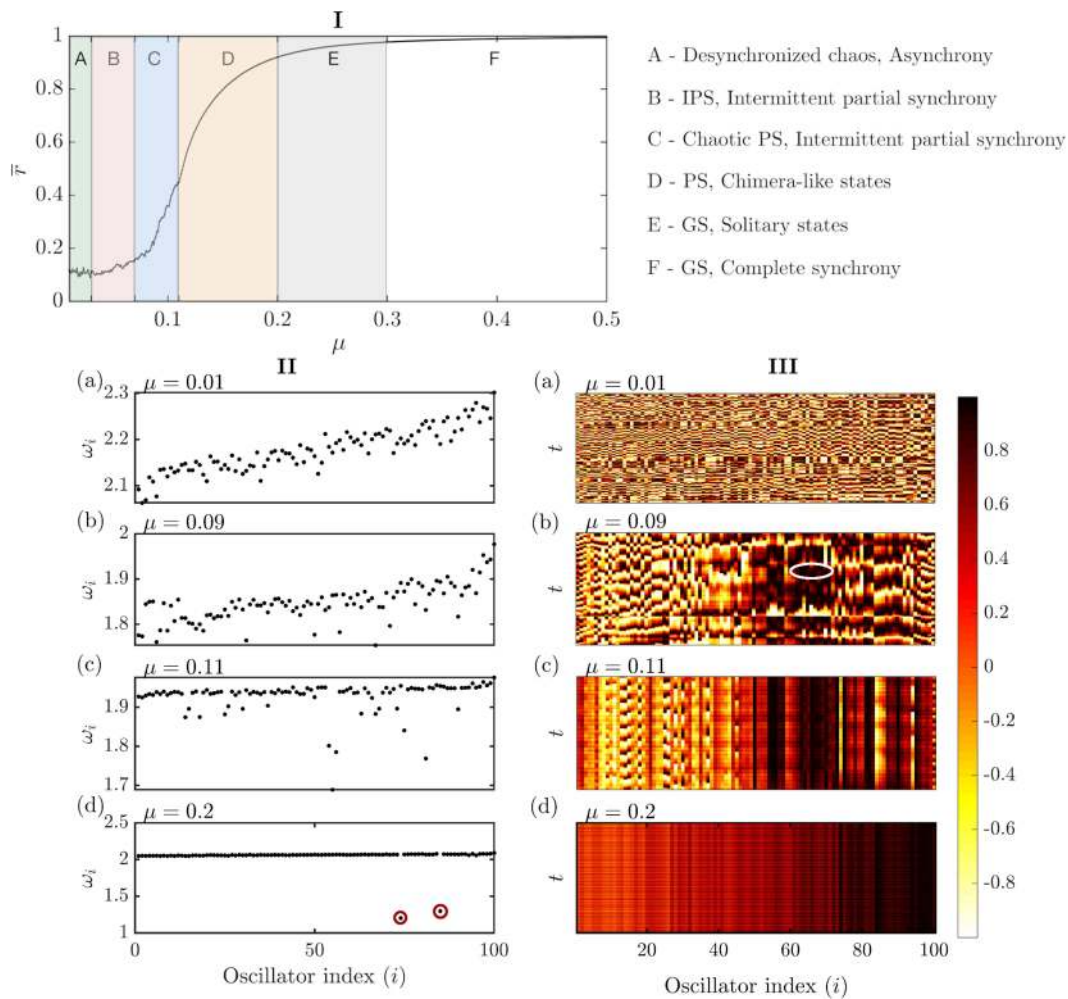


FIG. 5. I. Variation of \bar{v} with μ for different regimes during the synchronization transition from desynchronized chaos to synchronized order. The legend describes the synchronization state between v' and \bar{y}' followed by the spatiotemporal synchronization state among the Rössler oscillators. II(a)–(d) Mean phase velocities (ω_i) for the 100 Rössler oscillators at the coupling strengths $\mu = 0.01, 0.09, 0.11,$ and $0.2,$ respectively. III(a)–(d) Space time plots of $\cos(\theta_i)$, where θ_i represents the instantaneous phase difference between the i th Rössler oscillator and the chaotic VDP oscillator at $\mu = 0.01, 0.09, 0.11,$ and $0.2,$ respectively. The Rössler oscillators are ordered in the increasing order of their natural frequencies ω_i .

and 5-III(d)], we identify a solitary state where two oscillators [encircled in Fig. 5-II(d)] are not synchronized with the other 98 oscillators. We observe complete synchronization among the oscillators for $\mu > 0.3$.

We summarize the synchronization route between the chaotic Van der Pol oscillator (v') and the mean field of the grid of Rössler oscillators (\bar{y}') as the coupling strength is varied in Fig. 5-I. Simultaneously, we also describe the spatiotemporal synchronization route observed among the Rössler oscillators. Regime A corresponds to desynchronized chaos. Within regime B ($0.03 \leq \mu < 0.07$), v' and \bar{y}' are in the IPS state and there is intermittent partial synchrony among the Rössler oscillators. For higher coupling strengths, in regime C ($0.07 \leq \mu < 0.1$), v' and \bar{y}' are in the chaotic PS state and

there is intermittent partial synchrony among the Rössler oscillators. In regime D ($0.1 \leq \mu < 0.2$), v' and \bar{y}' are in the PS state and we observe the presence of chimera-like states among the Rössler oscillators. For higher coupling strengths of $0.2 \leq \mu < 0.3$ (in regime E), v' and \bar{y}' are in the GS state and we observe the presence of solitary states among the Rössler oscillators. Finally, regime F ($\mu \geq 0.3$) corresponds to the GS state between v' and \bar{y}' and complete synchrony among the Rössler oscillators. Thus, we uncover a spatiotemporal transition from desynchronized chaos to synchronized order via intermittent partial synchronization, chimera, and solitary states. A similar transition from desynchronized chaos to synchronized order via breathing chimera was observed in a thermoacoustic system during the onset of thermoacoustic instability.^{6,7}

IV. CONCLUSIONS

We reported a synchronization transition between a chaotic Van der Pol oscillator and the mean field of a Rössler system from desynchronized chaos followed by intermittent phase synchronization, chaotic phase synchronization, phase synchronization, and then to generalized synchronization. We detected a spatiotemporal transition from desynchronized chaos to global synchrony among the Rössler oscillators through the emergence of symmetry breaking states such as intermittent partial synchronization, chimera, and solitary states. The dynamics from the model is similar to those observed during the transition to oscillatory instabilities such as thermoacoustic, aeroacoustic, and aeroelastic instabilities in turbulent systems. Hence, simple models, such as the one we proposed, which exhibit a transition from desynchronized chaos to synchronized periodicity, can be used to depict the dynamics during the self-organization of turbulent flows. Since such oscillatory instabilities have detrimental consequences to the system, mitigating them is important. Hence, the model in our study paves the way to perform inexpensive numerical control experiments to arrive at strategies for suppressing synchronization, which could prevent such oscillatory instabilities in turbulent systems.

ACKNOWLEDGMENTS

We acknowledge DST, India, and DAAD, Germany, for funding the Indo-German joint project (F. No. DST/INT/FRG/DAAD/P-12/2017). We acknowledge support by the Office of Naval Research (ONR) Global (contract monitor: Dr. R. Kolar; Grant No. N62909-18-1). We thank Dr. Vishnu R. Unni for the discussions that aided in improving the manuscript.

APPENDIX A: CONVERGENCE OF DYNAMICS WITH NUMBER OF RÖSSLER OSCILLATIONS

We considered 100 Rössler oscillators in the model for analysis. In order to show convergence of results with respect to the number of oscillators, we study the variation of \bar{r} with μ for 100, 225, and 400 Rössler oscillators (Fig. 6). We observe a similar synchronization route and the onset of global synchrony at a coupling strength around $\mu = 0.2$. The slight differences can be attributed to the change in frequencies among the oscillators since they are assigned randomly from a Gaussian distribution with a mean of around 0.8 and a standard deviation of 0.05.

APPENDIX B: MODEL WITH THE GRID OF RÖSSLER OSCILLATORS BIDIRECTIONALLY COUPLED WITH CHAOTIC DUFFING OSCILLATOR

We show the generality of our findings which are valid for different pairs of dissimilar oscillators but not limited to Rössler-chaotic VDP system. We consider another model with the grid of 100 diffusively coupled Rössler oscillators bidirectionally coupled with a chaotic Duffing oscillator. The Rössler-chaotic

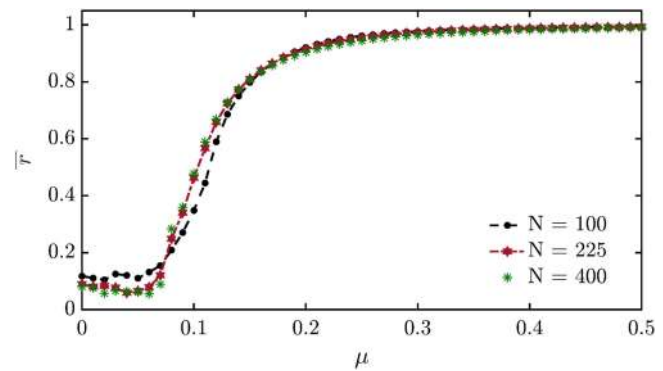


FIG. 6. Variation of \bar{r} with μ for $N = 100, 225,$ and 400 Rössler oscillators. We observe a similar variation in \bar{r} for various grid sizes.

Duffing system is given by Eqs. (B1) and (B2),

$$\begin{aligned} \dot{x}_i &= -w_i y_i - z_i, \\ \dot{y}_i &= w_i x_i + a y_i + \mu_{ny} (n - y_i) + \mu_{yy} \sum_{j \in \delta(y_i)} (y_j - y_i), \end{aligned} \quad (B1)$$

$$\dot{z}_i = b + z_i (x_i - c),$$

$$\dot{m} = n,$$

$$\dot{n} = m (1 - m^2) - 0.3n + 0.5 \cos 1.2t + \mu_{ym} \sum_{k=1}^N (y_k - n), \quad (B2)$$

where $a = 0.165$, $b = 0.2$, and $c = 10$ are the parameters of individual Rössler oscillator. $\delta(y_i)$ represents the nearest neighborhood of the i th Rössler oscillator and N represents the total number of Rössler oscillators. The ordinates of these oscillators are coupled to their neighbors within a distance of $\sqrt{2}$ units, with a coupling strength of μ_{yy} (intra-Rössler coupling). The natural frequencies of individual Rössler oscillators (w_i) are assigned randomly from a Gaussian distribution with a mean of around 0.8 and a standard deviation of 0.05. Equation (B2) represents the chaotic Duffing oscillator. The second coordinates of the Rössler system (\bar{y}) and the chaotic Duffing oscillator (n) are bidirectionally coupled with strengths of μ_{ny} and μ_{ym} , which corresponds to the influence of the Duffing oscillator on a Rössler oscillator and vice versa. We vary μ_{ym} and μ_{ny} as per the relation $\mu_{ym} = 1.2\mu_{ny}$. We use a proportional relationship between μ_{ny} and μ_{yy} as $\mu_{yy} = 0.1\mu_{ny}$. We observe a transition from chaos to limit cycle oscillations via intermittency as μ_{ny} is increased from 0 to 0.5.

Figure 7 shows a similar route of synchronization transition from desynchronized chaos to synchronized periodicity via intermittency in both the Rössler-chaotic Duffing and Rössler-chaotic VDP systems.

APPENDIX C: MULTIFRACTAL DETRENDED FLUCTUATION ANALYSIS

If the signal is $p(t)$ and N is the length of the signal, a mean subtracted cumulative signal is computed from $p(t)$.

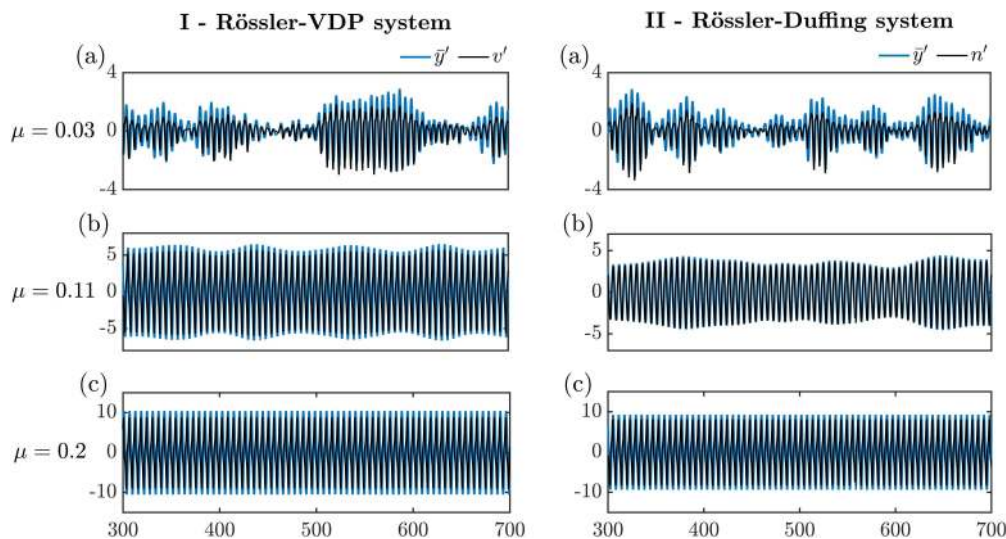


FIG. 7. I(a)–(c) Time series of the ordinate of chaotic VDP oscillator (v') and the mean field of the ordinate of the Rössler oscillators (\bar{y}') of the Rössler–VDP system obtained at $\mu = 0.03, 0.11,$ and 0.2 . II(a)–(c) Time series of the ordinate of chaotic Duffing oscillator (n') and the mean field of the ordinate of the Rössler oscillators (\bar{y}') of the Rössler–Duffing system obtained at $\mu = 0.03, 0.11,$ and 0.2 . We observe a similar transition in both the systems.

The new signal is then partitioned into N_s non-overlapping windows of equal size s . The local trends are detrended using a linear fit \bar{p} . To account for the scaling of fluctuations at multiple scales in the signal, a structure function (F_s^w) of order w and span s is defined as

$$F_s^w = \left(\frac{1}{N_s} \sum_{i=1}^{N_s} \left(\frac{1}{s} \sum_{i=1}^s (p_i - \bar{p})^2 \right)^{\frac{w}{2}} \right)^{\frac{1}{w}}. \quad (\text{C1})$$

The slope of the linear regime in the logarithmic plot of F_s^w vs various span sizes (s) gives the generalized Hurst exponent H^w of order w . The Hurst exponent corresponding to the correlation of the signal is the generalized Hurst exponent of order 2 (H^2). These generalized Hurst exponents can be represented using a spectrum of singularity exponents $f(\alpha)$ using the Legendre transformation, where α is a singularity exponent. The Legendre transform to obtain the singularity spectrum is given as⁴⁹

$$\begin{aligned} \tau_w &= wH^w - 1, \\ \alpha &= \frac{\partial \tau_w}{\partial w}, \\ f(\alpha) &= w\alpha - \tau_w. \end{aligned}$$

The multifractal spectrum is represented as the plot between $f(\alpha)$ and α . The width and skewness of the multifractal spectrum encode the information pertaining to the complexity of the signal.

REFERENCES

- ¹V. Nair, G. Thampi, and R. Sujith, *J. Fluid Mech.* **756**, 470 (2014).
- ²V. Nair and R. Sujith, *Int. J. Aeroacoust.* **15**, 312 (2016).
- ³J. Venkatramani, V. Nair, R. Sujith, S. Gupta, and S. Sarkar, *J. Fluid. Struct.* **61**, 376 (2016).
- ⁴S. A. Pawar, A. Seshadri, V. R. Unni, and R. Sujith, *J. Fluid Mech.* **827**, 664 (2017).
- ⁵A. Raaj, J. Venkatramani, and S. Mondal, *Chaos* **29**, 043129 (2019).
- ⁶S. Mondal, V. R. Unni, and R. Sujith, *J. Fluid Mech.* **811**, 659 (2017).
- ⁷S. A. Pawar, S. Mondal, N. B. George, and R. Sujith, *AIAA J.* **57**, 836 (2018).
- ⁸C. S. Peskin, *Mathematical Aspects of Heart Physiology* (Courant Institute of Mathematical Sciences, 1975).
- ⁹A. T. Winfree, *The Geometry of Biological Time* (Springer Science & Business Media, 2001), Vol. 12.
- ¹⁰S. Strogatz, *Sync: The Emerging Science of Spontaneous Order* (Penguin, UK, 2004).
- ¹¹S. Watanabe and S. H. Strogatz, *Physica D* **74**, 197 (1994).
- ¹²W. Wang, I. Z. Kiss, and J. Hudson, *Chaos* **10**, 248 (2000).
- ¹³I. Z. Kiss, Y. Zhai, and J. L. Hudson, *Science* **296**, 1676 (2002).
- ¹⁴H. Kori, C. G. Rusin, I. Z. Kiss, and J. L. Hudson, *Chaos* **18**, 026111 (2008).
- ¹⁵G. Filatrella, A. H. Nielsen, and N. F. Pedersen, *Eur. Phys. J. B* **61**, 485 (2008).
- ¹⁶A. E. Motter, S. A. Myers, M. Anghel, and T. Nishikawa, *Nat. Phys.* **9**, 191 (2013).
- ¹⁷S. H. Strogatz, *Physica D* **143**, 1 (2000).
- ¹⁸H. Hong and S. H. Strogatz, *Phys. Rev. Lett.* **106**, 054102 (2011).
- ¹⁹A. T. Winfree, *Science* **298**, 2336 (2002).
- ²⁰M. J. Panaggio and D. M. Abrams, *Nonlinearity* **28**, R67 (2015).
- ²¹P. Jaros, S. Brezetsky, R. Levchenko, D. Dudkowski, T. Kapitaniak, and Y. Maistrenko, [arXiv:1703.06950](https://arxiv.org/abs/1703.06950) (2017).
- ²²J. Chen, K. Wong, and J. Shuai, *Phys. Rev. E* **66**, 056203 (2002).
- ²³R. Karnatak, R. Ramaswamy, and A. Prasad, *Chaos* **19**, 033143 (2009).
- ²⁴S. Chaurasia and S. Sinha, *Nonlinear Dyn.* **87**, 159 (2017).
- ²⁵V. Nair, G. Thampi, S. Karuppusamy, S. Gopalan, and R. Sujith, *Int. J. Spray Combust. Dyn.* **5**, 273 (2013).
- ²⁶J. Venkatramani, V. Nair, R. Sujith, S. Gupta, and S. Sarkar, *J. Sound Vib.* **386**, 390 (2017).
- ²⁷M. P. Juniper and R. Sujith, *Annu. Rev. Fluid Mech.* **50**, 661 (2018).
- ²⁸Y. C. Fung, *An Introduction to the Theory of Aeroelasticity* (Courier Dover Publications, 2008).
- ²⁹A. K. Dutta, G. Ramachandran, and S. Chaudhuri, *Phys. Rev. E* **99**, 032215 (2019).
- ³⁰C. Meena, K. Murali, and S. Sinha, *Int. J. Bifurc. Chaos* **26**, 1630023 (2016).

- ³¹Y. Ku and X. Sun, *J. Franklin Inst.* **327**, 197 (1990).
- ³²V. Godavarthi, S. A. Pawar, V. R. Unni, R. Sujith, N. Marwan, and J. Kurths, *Chaos* **28**, 113111 (2018).
- ³³H. G. Schuster and W. Just, *Deterministic Chaos: An Introduction* (John Wiley & Sons, 2006).
- ³⁴X. Han, M. Wei, Q. Bi, and J. Kurths, *Phys. Rev. E* **97**, 012202 (2018).
- ³⁵P. F. Panter, *Modulation, Noise and Spectral Analysis: Applied to Information Transmission* (McGraw-Hill, 1965).
- ³⁶J. Eckmann, S. O. Kamphorst, and D. Ruelle, *Europhys. Lett.* **4**, 973 (1987).
- ³⁷M. C. Romano, M. Thiel, J. Kurths, I. Z. Kiss, and J. Hudson, *Europhys. Lett.* **71**, 466 (2005).
- ³⁸B. Goswami, G. Ambika, N. Marwan, and J. Kurths, *Physica A* **391**, 4364 (2012).
- ³⁹M. Lakshmanan and D. V. Senthilkumar, *Dynamics of Nonlinear Time-Delay Systems* (Springer Science & Business Media, 2011).
- ⁴⁰L. Lacasa, B. Luque, F. Ballesteros, J. Luque, and J. C. Nuno, *Proc. Natl. Acad. Sci. U.S.A.* **105**, 4972 (2008).
- ⁴¹J. Zhang and M. Small, *Phys. Rev. Lett.* **96**, 238701 (2006).
- ⁴²M. Murugesan and R. Sujith, *J. Fluid Mech.* **772**, 225 (2015).
- ⁴³B. B. Mandelbrot, *The Fractal Geometry of Nature* (W.H. Freeman, New York, 1983), Vol. 173.
- ⁴⁴B. Mandelbrot, *Science* **156**, 636 (1967).
- ⁴⁵B. B. Mandelbrot, *Multifractals and 1/f Noise: Wild Self-Affinity in Physics (1963–1976)* (Springer, 2013).
- ⁴⁶V. R. Unni and R. Sujith, *J. Fluid Mech.* **784**, 30 (2015).
- ⁴⁷Y. Kuramoto, *Chemical Oscillations, Waves, and Turbulence* (Courier Corporation, 2003).
- ⁴⁸I. Omelchenko, E. Omel'chenko, P. Hövel, and E. Schöll, *Phys. Rev. Lett.* **110**, 224101 (2013).
- ⁴⁹R. K. Zia, E. F. Redish, and S. R. McKay, *Am. J. Phys.* **77**, 614 (2009).